electronics

MDPI

Article

A Sub/Super-Synchronous Oscillation Localization Method Based on Graph Attention Network with Physical Feature Embedding

Buqing Deng [1], Rong Ye [1], Luojia Yang [2], Jianghui Li [1], Jiajian Lin [1], Shilin Gao [2,*] and Chenhao Guan [1]

[1] Economic and Technical Research Institute, State Grid Fujian Electric Power Co., Ltd., Fuzhou 350013, China; deng_buqing@fj.sgcc.com.cn (B.D.); ye_rong@fj.sgcc.com.cn (R.Y.); li_jianghui@fj.sgcc.com.cn (J.L.); lin_jiajian@fj.sgcc.com.cn (J.L.); guan_chenhao@fj.sgcc.com.cn (C.G.)

[2] College of Electrical Engineering, Sichuan University, Chengdu 610065, China; 2024223030028@stu.scu.edu.cn

* Correspondence: gaoshilin@scu.edu.cn; Tel.: +86-15901063704

Abstract

With the continuous increase in the capacity of grid-connected new energy sources such as wind and photovoltaic power, the issues of sub-synchronous oscillation and super-synchronous oscillation caused by the interaction between power electronic devices and the grid have become increasingly prominent. Therefore, accurately localizing online oscillation sources is of great importance for preventing the expansion of accidents. In this paper, a modal parameter identification method is first proposed. By selecting the real part of the synchrophasor as the characteristic quantity, the precise decoupling and identification of Sub/Super-SO modal parameters are realized. On this basis, a physical feature-embedded graph attention network localization method is proposed, in which the high-precision modal parameters obtained from identification are embedded as physical features into graph nodes, and the attention mechanism is used to adaptively learn the oscillation propagation patterns in the grid topology. Finally, simulation verification based on the IEEE 14-bus system demonstrates that the proposed method can effectively achieve accurate localization of oscillation sources.

Keywords: sub/super-synchronous oscillation; wide area measurement system; modal parameter identification; graph attention network; oscillation localization

1. Introduction

Under the "dual-carbon" strategic goals, the penetration of renewable energy generation in power system generation structures has been steadily increasing, accompanied by the large-scale integration of power electronic devices [1,2]. In power-electronics-dominated power systems, stability problems exhibit more diverse frequency-domain and dynamic characteristics, and can be classified from the perspectives of oscillation frequency, interaction mechanism, and device–grid coupling behavior [3]. As a result, sub-synchronous oscillation (Sub-SO) and super-synchronous oscillation (Super-SO) issues have become increasingly prominent. Sub/Super-SO is typically excited by the interaction between specific oscillatory modes of the power system and power electronic devices. Such oscillations often originate from local disturbances and gradually propagate across the entire network [4,5], with oscillation energy spreading widely, thereby posing significant challenges to system stability analysis and oscillation suppression [6–9]. Therefore, it is of great theoretical and

Check for updates

Academic Editor: Pasquale De Falco

Received: 7 May 2026
Revised: 16 June 2026
Accepted: 20 June 2026
Published: 23 June 2026

Copyright: © 2026 by the authors. Licensee MDPI, Basel, Switzerland. This article is an open access article distributed under the terms and conditions of the Creative Commons Attribution (CC BY) license.

practical significance to research the online parameter identification and source localization of Sub/Super-SO.

The frequent occurrence of Sub/Super-SO highlights the increasing importance of monitoring capabilities in ensuring the secure and stable operation of power systems. To address this, wide area measurement systems (WAMSs) based on phasor measurement units (PMUs) have been widely deployed in power system operation and dispatch. WAMSs enable comprehensive monitoring and dynamic awareness of various components of the power system, allowing operators to rapidly obtain system-wide information during faults or disturbances, thereby enhancing system operational stability [10].

Research on oscillation analysis and source localization based on WAMSs has attracted increasing attention. From the perspective of data sources, existing Sub/Super-SO identification methods can be broadly classified into two categories. The first category relies on data generated from simulation models or analytical signal models. For example, signal-parameter-estimation techniques have been introduced into electromagnetic transient simulation and dynamic signal analysis. Gao et al. proposed an ESPRIT-based interface method for the co-simulation of conventional electromagnetic transient models and shifted-frequency electromagnetic transient models, in which the frequency, amplitude, and phase of instantaneous signals are estimated to construct analytical signals for accurate interface conversion [11]. The second category relies on measured data collected from practical power systems, which can be further divided into PMU-substation-based methods and WAMS-control-center-based methods. PMU-substation-based methods utilize instantaneous measurements to perform modal parameter identification, for which the related theoretical studies are relatively mature [8,12,13]. In contrast, WAMS-control-center-based methods rely on synchronized phasor data collected at the WAMS control center. By aggregating low-frequency synchrophasor measurements from key nodes, the WAMS control center enables the extraction of global information of Sub/Super-SO, thereby facilitating wide-area monitoring [14,15].

However, existing parameter identification methods still exhibit certain limitations. On the one hand, constrained by the Nyquist sampling theorem, they are generally limited to identifying only Sub-SO modes. On the other hand, these methods typically require predefined signal models, making it difficult to accurately identify oscillation modes containing multiple pairs of coupled Sub/Super-SO components [16]. In summary, although oscillation monitoring based on control-center synchrophasor data is still in its early stage, its global observability provides important foundational support for subsequent oscillation source localization and mitigation.

Oscillation source localization methods based on WAMSs can be broadly classified into two categories: mechanism-based methods and artificial intelligence-based methods. Mechanism-based approaches generally locate oscillation sources by analyzing system models, oscillation energy, modal energy, or transient energy flow. For example, recent studies have proposed refined energy-based traceability methods and multivariate variational mode decomposition-based transient energy flow methods for locating SSO sources in renewable-energy-integrated power systems [17,18]. In addition, forced-oscillation source localization methods that account for grid-forming wind turbines and harmonic/interharmonic interference have also been developed [19]. These methods have strong physical interpretability, but their performance may be affected by nonlinear operating conditions, noise interference, and complex multi-mode oscillation coupling.

Both analytical and numerical methods are model-based approaches with strong physical interpretability. However, they exhibit limited capability in handling nonlinear conditions and are less suitable for scenarios with high uncertainty.

Compared with mechanism-based oscillation source localization methods, artificial intelligence (AI)-based approaches exhibit lower dependence on system models and stronger robustness to noise, making them more suitable for oscillation source localization in modern power systems. Recent studies have applied deep learning and attention-based models to oscillation identification, classification, and localization. For instance, compressed sensing combined with graph attention networks has been used for wideband oscillation localization by incorporating power grid topology and node feature information [20]. Multimodal attention-based fusion networks have also been developed for wideband oscillation classification by jointly extracting image-domain and time-series features [21]. Moreover, deep reinforcement learning has been applied to time-varying parameter identification in grid-connected renewable power generation systems, demonstrating its capability in handling nonlinear dynamics and multi-parameter coupling [22]. As for methods based on WAMS, Ref. [23] proposed a PMU data-driven method for locating forced oscillation sources, which constructs a measurement matrix and employs maximum likelihood estimation to identify system dynamic characteristics and the oscillation source location simultaneously. Refs. [24,25] introduced compressive sensing techniques to improve the accuracy and robustness of data transmission from PMUs to the control center under bandwidth constraints, thereby enabling online oscillation source localization.

However, existing purely data-driven methods generally rely on high-frequency waveform data from PMU substations, which not only leads to high data dimensionality, but also lacks physical interpretability, making them difficult to be directly applied to synchrophasor data at the WAMS control center for online monitoring. In addition, these methods often neglect the constraints imposed by power system topology on oscillation propagation and fail to effectively exploit the spatial correlations among nodes.

To address the above issues, this paper proposes a method for oscillation parameter identification based on synchrophasor data from the WAMS control center, combined with physical feature embedding and graph attention networks for oscillation source localization. The contributions of this paper are summarized as follows:

(1) A synchrophasor-based Sub/Super-SO modal parameter identification method is developed for WAMS control-center data, which addresses the difficulty of identifying coupled Sub/Super-SO components under spectral aliasing conditions.
(2) The identified modal parameters, including amplitude, damping factor, and phase, are embedded into graph nodes as physically interpretable features, and a graph attention network-based localization framework is constructed to incorporate power grid topology and learn the spatial propagation characteristics of oscillations, thereby avoiding the direct use of high-dimensional raw waveform data.

The remainder of this paper is organized as follows. Section 2 introduces the proposed synchrophasor-based Sub/Super-SO modal parameter identification method. Section 3 presents the oscillation source localization method based on physical feature embedding and graph attention networks. Section 4 verifies the effectiveness of the proposed identification and localization methods using a modified IEEE 14-bus system and compares the proposed method with representative localization approaches. Finally, Section 5 concludes the paper.

2. Oscillation Modal Parameter Identification Based on Synchrophasors

Sub-SO in power systems is an instability phenomenon caused by the interaction between the system's electrical characteristics and control loops or mechanical components. Existing studies on Sub-SO modal parameter identification often fail to adequately consider the influence of Super-SO components and their coupling with Sub-SO components on the identification results. To address this issue, this section proposes a Sub/Super-SO

modal parameter identification method that fully exploits the real-time and wide-area synchronization advantages of synchrophasor data.

2.1. Spectral Aliasing of Super-SO

The spectral aliasing considered in this paper refers to the phenomenon that during PMU sampling, when the sampling frequency does not satisfy the Nyquist sampling theorem, high-frequency signal components are folded and mapped into the low-frequency band, thereby overlapping with the low-frequency components in the spectrum. Essentially, this phenomenon is a frequency ambiguity effect caused by undersampling.

When Sub/Super-SO occurs, the system voltage and current signals can be represented as a superposition of multiple oscillatory modes, and the corresponding mathematical model can be expressed as:

$$x(t) = \sum_{i=0}^{2} A_i e^{\alpha_i t} \cos(2\pi f_i t + \varphi_i) \tag{1}$$

where $x(t)$ denotes the voltage or current signal, which mainly consists of three components: the fundamental component, the Sub-SO component, and the Super-SO component. The frequencies of the Sub-SO and Super-SO components are coupled, satisfying $f_1 + f_2 = 2f_N$. A_i, α_i, f_i, and φ_i represent the amplitude, damping factor, frequency, and phase of the i-th component, respectively.

According to Ref. [26], the synchrophasor $X(r)$ of the voltage and current signals during Sub/Super-SO can be derived. $X(r)$ contains both fundamental and Sub/Super-SO components, and these components are linearly superimposed.

$$\begin{aligned} X(r) &= \frac{1}{2N_p} \sum_{i=0}^{2} A_i \mathrm{e}^{r\frac{\alpha_i}{f_p}} \left(\mathrm{e}^{\mathrm{j}(2\pi r \frac{f_i}{f_p} + \varphi_i)} H_{i1} \mathrm{e}^{\mathrm{j}\theta_{i1}} + \mathrm{e}^{-\mathrm{j}(2\pi r \frac{f_i}{f_p} + \varphi_i)} H_{i2} \mathrm{e}^{-\mathrm{j}\theta_{i2}} \right) \\ &= \frac{1}{2N_p} \sum_{i=0}^{2} A_i \mathrm{e}^{\frac{\alpha_i}{f_p} r} \left(F_{i1} \cos(2\pi r \frac{f_i}{f_p} + \varphi_i + \phi_{i1}) + j F_{i2} \sin(2\pi r \frac{f_i}{f_p} + \varphi_i + \phi_{i2}) \right) \end{aligned} \tag{2}$$

where f_p denotes the PMU sampling frequency, f_N represents the fundamental frequency of the system, $N_p = f_p/f$, $F_{i1} = \sqrt{{H_{i1}}^2 + {H_{i2}}^2 + 2H_{i1}H_{i2}\cos(\theta_{i1} - \theta_{i2})}$, and $\phi_{i1} = \arctan\left(\frac{H_{i1}\sin(\theta_{i1}) + H_{i2}\sin(\theta_{i2})}{H_{i1}\cos(\theta_{i1}) + H_{i2}\cos(\theta_{i2})}\right)$.

According to Equation (2), the time-domain characteristics of Sub/Super-SO exhibit a clear correspondence with the real and imaginary parts of the synchrophasor. Although the Super-SO component cannot be directly resolved due to the limitations of the reporting rate of synchrophasors and the sampling theorem, its information is still implicitly contained in the synchrophasor data. To this end, this section first detects the presence of Sub/Super-SO components based on the real part of the synchrophasor. On this basis, the fundamental component is decoupled from the Sub/Super-SO components, enabling the identification of Sub/Super-SO modal parameters.

PMU substations transmit data at a reporting rate of f_r, and thus the synchrophasor sequence $X_n(m)$ received at the control center can be expressed as:

$$X_n(m) = X\left(mf_p/f_r\right) \tag{3}$$

Substituting Equation (3) into Equation (2):

$$\begin{aligned} X_n(m) &= \frac{1}{2N_p}\sum_{i=0}^{2} A_i e^{m\frac{\alpha_i}{f_r}}\left(e^{j(2\pi m\frac{f_i}{f_r}+\varphi_i)}H_{i1}e^{j\theta_{i1}} + e^{-j(2\pi m\frac{f_i}{f_r}+\varphi_i)}H_{i2}e^{-j\theta_{i2}}\right) \\ &= \frac{1}{2N_p}\sum_{i=0}^{2} A_i e^{m\frac{\alpha_i}{f_r}}\left(F_{i1}\cos(2\pi m\frac{f_i}{f_r}+\varphi_i+\phi_{i1}) + jF_{i2}\sin(2\pi m\frac{f_i}{f_r}+\varphi_i+\phi_{i2})\right) \end{aligned} \tag{4}$$

The real part of the synchrophasor is given by:

$$\mathrm{Re}(X_n) = |X_n(m)|\cos(\lambda) = \frac{1}{2N_p}\sum_{i=0}^{2} A_i F_{i1} e^{m\frac{\alpha_i}{f_r}}\left(\cos\left(\frac{2\pi m f_i}{f_r}+\varphi_i+\phi_{i1}\right)\right) \tag{5}$$

When $f_r = 2f_N$, Equation (5) can be simplified as:

$$\begin{aligned} \mathrm{Re}(X_n) = \tfrac{1}{2N_p}&\left(A_0F_{01}e^{m\frac{\alpha_0}{f_r}}\cos(2\pi m\tfrac{f_0}{f_r}+\varphi_0+\phi_{01}) + A_1F_{11}e^{m\frac{\alpha_1}{f_r}}(\cos(2\pi m\tfrac{f_1}{f_r}+\varphi_1+\phi_{11})\right. \\ &\left.+A_2F_{21}e^{m\frac{\alpha_2}{f_r}}(\cos(2\pi m\tfrac{f_1}{f_r}+\varphi_2+\phi_{21}))\right) \end{aligned} \tag{6}$$

It can be seen from Equation (6) that when $f_r = 2f_N$, the Super-SO and Sub-SO components overlap in the frequency domain. Therefore, under this condition, if a Sub-SO component is detected through spectral analysis of the real part of the synchrophasor, the corresponding time-domain oscillation may fall into one of the following cases:

1. Only Sub-SO exists;
2. Only Super-SO exists;
3. Coupled Sub/Super-SO oscillations exist.

To improve the accuracy of frequency estimation, an interpolated discrete Fourier transform (interpolated discrete Fourier transform, IpDFT) is further employed to obtain the precise frequencies of the Sub/Super-SO components.

2.2. Decoupling and Parameter Identification of Sub/Super-SO Components

As can be seen from Equation (4), each frequency component can be decomposed into two components rotating at angular frequencies $\pm 2\pi f^i$, as shown in Figure 1.

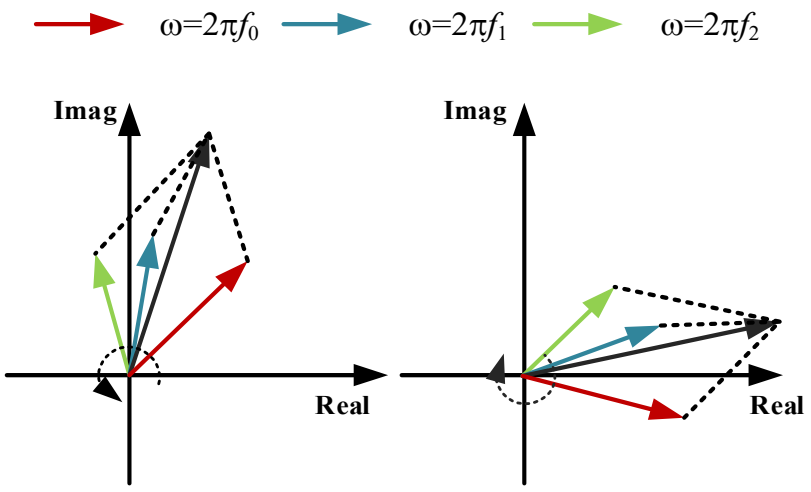


Figure 1. Rotational characteristics of synchronous phasors. The colored arrows represent phasor components at different angular frequencies, and the black solid arrows denote the resultant vectors of the colored components. The black dotted arrows indicate their directions of rotation.

Equation (4) can be rewritten in matrix form as:

$$\boldsymbol{B}\begin{bmatrix} A_0H_{01}e^{j(\varphi_0+\theta_{01})} \\ A_0H_{02}e^{-j(\varphi_0+\theta_{02})} \\ A_1H_{11}e^{j(\varphi_1+\theta_{11})} \\ A_1H_{12}e^{-j(\varphi_1+\theta_{12})} \\ A_2H_{21}e^{j(\varphi_2+\theta_{21})} \\ A_2H_{22}e^{-j(\varphi_2+\theta_{22})} \end{bmatrix} = \begin{bmatrix} X_n(m) \\ X_n(m+1) \\ X_n(m+2) \\ X_n(m+3) \\ X_n(m+4) \\ X_n(m+5) \end{bmatrix} \tag{7}$$

where the matrix $\boldsymbol{B}$ is constructed from rotation factors $e^{\frac{j2\pi f}{f_r}}$ and is used to characterize the forward and backward rotational properties of each component in the synchrophasor, with its specific form given in Equation (8).

$$\boldsymbol{B} = \frac{1}{2N_p}\begin{bmatrix} 1 & 1 & 1 & 1 & 1 & 1 \\ e^{\frac{\alpha_0+j2\pi f_0}{f_r}} & e^{\frac{\alpha_0-j2\pi f_0}{f_r}} & e^{\frac{\alpha_1+j2\pi f_0}{f_r}} & e^{\frac{\alpha_1-j2\pi f_0}{f_r}} & e^{\frac{\alpha_2+j2\pi f_0}{f_r}} & e^{\frac{\alpha_2-j2\pi f_0}{f_r}} \\ e^{2\frac{\alpha_0+j2\pi f_0}{f_r}} & e^{2\frac{\alpha_0-j2\pi f_0}{f_r}} & e^{2\frac{\alpha_1+j2\pi f_0}{f_r}} & e^{2\frac{\alpha_1-j2\pi f_0}{f_r}} & e^{2\frac{\alpha_2+j2\pi f_0}{f_r}} & e^{2\frac{\alpha_2-j2\pi f_0}{f_r}} \\ e^{3\frac{\alpha_0+j2\pi f_0}{f_r}} & e^{3\frac{\alpha_0-j2\pi f_0}{f_r}} & e^{3\frac{\alpha_1+j2\pi f_0}{f_r}} & e^{3\frac{\alpha_1-j2\pi f_0}{f_r}} & e^{3\frac{\alpha_2+j2\pi f_0}{f_r}} & e^{3\frac{\alpha_2-j2\pi f_0}{f_r}} \\ e^{4\frac{\alpha_0+j2\pi f_0}{f_r}} & e^{4\frac{\alpha_0-j2\pi f_0}{f_r}} & e^{4\frac{\alpha_1+j2\pi f_0}{f_r}} & e^{4\frac{\alpha_1-j2\pi f_0}{f_r}} & e^{4\frac{\alpha_2+j2\pi f_0}{f_r}} & e^{4\frac{\alpha_2-j2\pi f_0}{f_r}} \\ e^{5\frac{\alpha_0+j2\pi f_0}{f_r}} & e^{5\frac{\alpha_0-j2\pi f_0}{f_r}} & e^{5\frac{\alpha_1+j2\pi f_0}{f_r}} & e^{5\frac{\alpha_1-j2\pi f_0}{f_r}} & e^{5\frac{\alpha_2+j2\pi f_0}{f_r}} & e^{5\frac{\alpha_2-j2\pi f_0}{f_r}} \end{bmatrix} \tag{8}$$

If $\boldsymbol{B}$ is full rank, Equation (7) is solvable, and the solution corresponds to the modal parameters of the Sub/Super-SO components. However, the damping factors associated with matrix $\boldsymbol{B}$ components remain unidentified. To address this issue, an iterative strategy is introduced in this section to identify the damping factors. Finally, the remaining modal parameters are obtained by combining the frequency identification results from the previous section.

First, initial values of the damping factors for each mode are assigned, based on which an initial iterative matrix is constructed. Suppose that N_r synchrophasor samples are obtained within 1 s; then, according to Equation (7), a system of equations containing N_r-5 equations can be established. Denote the solution of this system as $\eta(m)$, and take its magnitude:

$$|\eta(m)| = \begin{bmatrix} A_0(m)H_{01} \\ A_0(m)H_{02} \\ A_1(m)H_{11} \\ A_1(m)H_{12} \\ A_2(m)H_{21} \\ A_2(m)H_{22} \end{bmatrix} \tag{9}$$

where m = 0, 1, 2, …, N_r-5.

At this stage, the fundamental component and the Sub/Super-SO components have been decoupled. Taking the logarithm of $|A_i(m)H_{i1}|$, i = 0, 1, 2… and performing linear fitting, the slope a of the fitted line corresponds to the damping factor α. Taking $|A_0(m)H_{i1}|$ as an example:

$$\ln(|A_0(m)H_{01}|) = am + b \tag{10}$$

The estimated damping factors associated with each component are incorporated into matrix $\boldsymbol{B}$ for iterative matrix updating, and the above solving and fitting procedures are repeated. The iteration is terminated when the difference between the damping factors obtained in two consecutive iterations is less than 0.1%, and the results from the final iteration are taken as the identified parameters.

It should be noted that the proposed method is based on solving a system of linear equations, and its applicability requires the initial matrix $\boldsymbol{B}$ to be of full rank. As shown in Equation (8), $\boldsymbol{B}$ is a Vandermonde matrix. According to the property of a Vandermonde matrix, $\boldsymbol{B}$ is full rank only when the rotation factors corresponding to different modal components are mutually distinct. If two rotation factors are identical, the corresponding two columns of $\boldsymbol{B}$ become linearly dependent, and the modal components cannot be uniquely decoupled. Therefore, the solvability of Equation (7) depends on whether the selected reporting or equivalent sampling rate can make the rotation factors of different components distinguishable.

When $f_r = 100$ Hz $= 2f_N$, the real part of the synchrophasor is suitable for detecting the spectral overlap between Sub-SO and Super-SO components. However, this reporting rate may also cause degeneracy in the decoupling matrix. For example, for a coupled Sub/Super-SO pair satisfying $f_1 + f_2 = 2f_N = f_r$, the rotation factors $e^{j2\pi f_1/f_r}$ and $e^{j2\pi f_2/f_r}$ become identical. In this case, the corresponding columns of matrix B become linearly dependent, and the two modal components cannot be uniquely decoupled.

Therefore, this section proposes a resampling scheduling strategy for synchrophasor data. As illustrated in Figure 2, the PMU reporting rate is kept at 100 Hz throughout the whole observation period. The synchrophasor data in the first second are directly used for oscillation detection and frequency estimation, while the synchrophasor data in the second second are resampled from 100 Hz to an equivalent 80 Hz sequence at the WAMS control center for component decoupling and parameter identification. In this way, the proposed method does not require dynamic adjustment of the PMU reporting rate, and the required equivalent 80 Hz sequence is generated only through data preprocessing.

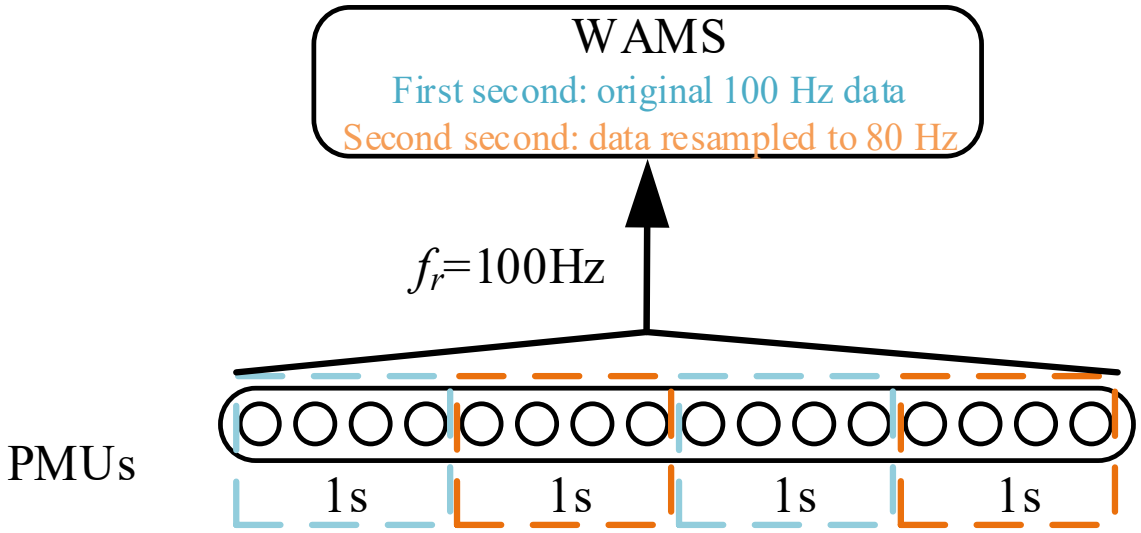


Figure 2. Resampling-based synchrophasor preprocessing scheme.

Since $f_1 + f_2$ is no longer equal to the equivalent reporting rate in the second second, the corresponding rotation factors become distinguishable, and matrix $\boldsymbol{B}$ satisfies the full-rank condition under the identified modal frequencies.

2.3. Sub/Super-SO Detection and Modal Parameter Identification Algorithm

This section adopts a 2 s period and utilizes voltage or current synchrophasor data to detect the Sub/Super-SO components and identify their modal parameters. The procedure is as follows:

1. During the first second, synchrophasor data are acquired at a reported rate of f_r = 100 Hz. The real component of the synchrophasor is adopted as the feature, and a discrete Fourier transform (DFT) is applied to determine whether Sub-SO components are present;
2. If Sub-SO components are detected, the IpDFT method is employed to accurately estimate their frequencies. Based on the frequency coupling relationship, the possible frequencies of the corresponding Super-SO components are then determined;
3. Using the identified frequencies of the Sub/Super-SO components, the initial matrix is constructed. Meanwhile, based on the synchrophasor data resampled at 80 Hz during the second second, the linear equation system in Equation (9) is solved to obtain the magnitude of the solution $|\eta(\mathrm{m})|$. Finally, the amplitudes and damping coefficients are determined using the approach outlined in Section 2.2.

3. Oscillation Source Localization via Graph Attention Networks with Physical Feature Embedding

3.1. Graph Construction and Physical Feature Embedding of Power Systems

Power systems exhibit well-defined topological structures and can be abstracted as a graph model $G = (V, E)$. In this representation, generator units and key substations are modeled as the node set V, while transmission lines are represented as the edge set E. The connectivity among nodes is described by the adjacency matrix A, enabling a digital representation of the power system topology.

Unlike conventional data-driven methods that directly use high-dimensional raw data, this paper employs the oscillation modal parameters identified in Section 1 as input features of graph nodes, thereby achieving an effective integration of physical knowledge and data-driven modeling. For node k, the input feature vector x_k is defined as:

$$x_k = \begin{bmatrix} a_k, & A_k, & \varphi_k \end{bmatrix} \tag{11}$$

where α_k, A_k, and φ_k denote the damping factor, amplitude, and phase of the oscillatory component at node k, respectively, as obtained from the identification results. The damping factor characterizes the damping property of the oscillation and serves as a key indicator of system stability; the amplitude reflects the distribution of disturbance energy; and the phase represents the propagation delay and relative position of the oscillation within the network.

The construction of this feature vector avoids the direct use of high-dimensional, noisy raw data, thereby significantly reducing model complexity while endowing the input features with clear physical interpretability.

3.2. Localization Output of Oscillation Sources

Graph attention networks (GATs) can automatically learn the contributions of different transmission lines to oscillation propagation in the power grid through the attention mechanism. If a node exhibits significant source-related characteristics, such as strong negative damping, its influence on neighboring nodes will be reflected in the attention weights, thereby forming a differentiated information propagation pattern over the graph structure. The GAT-based oscillation source localization process mainly consists of two stages, namely feature extraction and probability output. The block diagram of a GAT is shown in Figure 3.

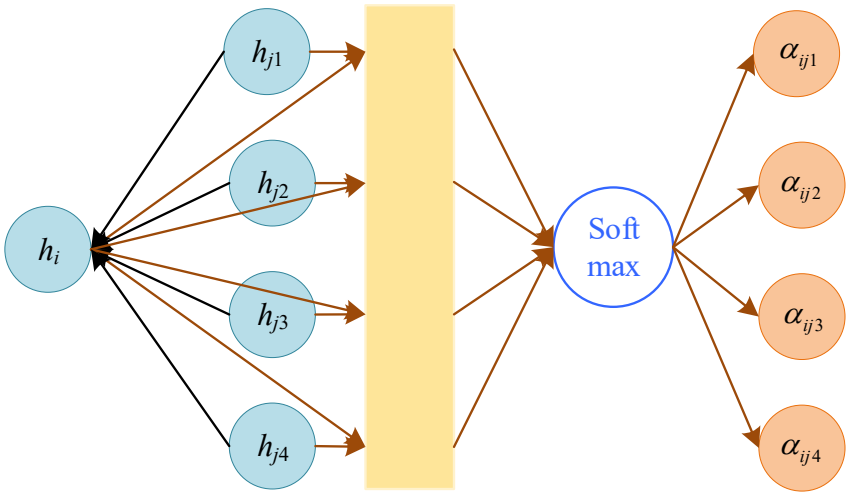


Figure 3. The block diagram of a GAT.

First, the attention coefficients between nodes are computed. For an arbitrary node i and its neighboring node $j \in N(i)$, the GAT computes the correlation coefficient between them through a learnable linear transformation and an attention mechanism.

$$e_{ij} = \text{leakyReLU}\left(\boldsymbol{a}^T \left[\boldsymbol{W}\boldsymbol{h}_i \| \boldsymbol{W}\boldsymbol{h}_j\right]\right) \tag{12}$$

where $\boldsymbol{h}_i$, $\boldsymbol{h}_j$ denote the input feature vectors of nodes I and j, respectively; $\boldsymbol{W}$ is the shared linear transformation weight matrix; $\boldsymbol{a}$ is the weight vector of a single-layer feedforward neural network in the attention mechanism; $\|$ represents the vector concatenation operation; and LeakyReLU is the nonlinear activation function.

Next, to ensure the comparability of the coefficients, the Softmax function is applied to normalize the attention coefficients, yielding the attention weight α_{ij}, of node j with respect to node i:

$$\alpha_{ij} = \frac{\exp\left(e_{ij}\right)}{\sum\limits_{k \in N(i)} \exp\left(e_{ij}\right)} \tag{13}$$

At the physical level, the weight α_{ij} reflects the coupling strength of oscillation energy or features propagating along transmission lines. If node j s an oscillation source, its distinctive physical characteristics, such as negative damping divergence, will result in higher attention weights during the aggregation of neighboring node features. Subsequently, the computed attention weights are used to perform weighted aggregation of neighboring features, and the high-level representation $\boldsymbol{h}_i'$ of node i is updated through a nonlinear activation function:

$$\boldsymbol{h}_i' = \sigma\left(\sum_{j \in N(i)} \alpha_{ij} \boldsymbol{W}\boldsymbol{h}_i\right) \tag{14}$$

where σ(·) denotes the nonlinear activation function (typically chosen as ELU). By stacking multiple graph attention layers, the physical features of oscillation-source nodes are propagated and progressively enhanced across the power grid topology, enabling the network to capture global oscillation distribution patterns.

Finally, the high-level node features produced by the GAT are fed into a fully connected layer, followed by a Softmax classifier to compute the probability that each node belongs to the oscillation source class. The node with the highest probability is identified as the oscillation source, thereby achieving accurate localization of Sub/Super-SO sources. The detailed workflow is shown in Figure 4.

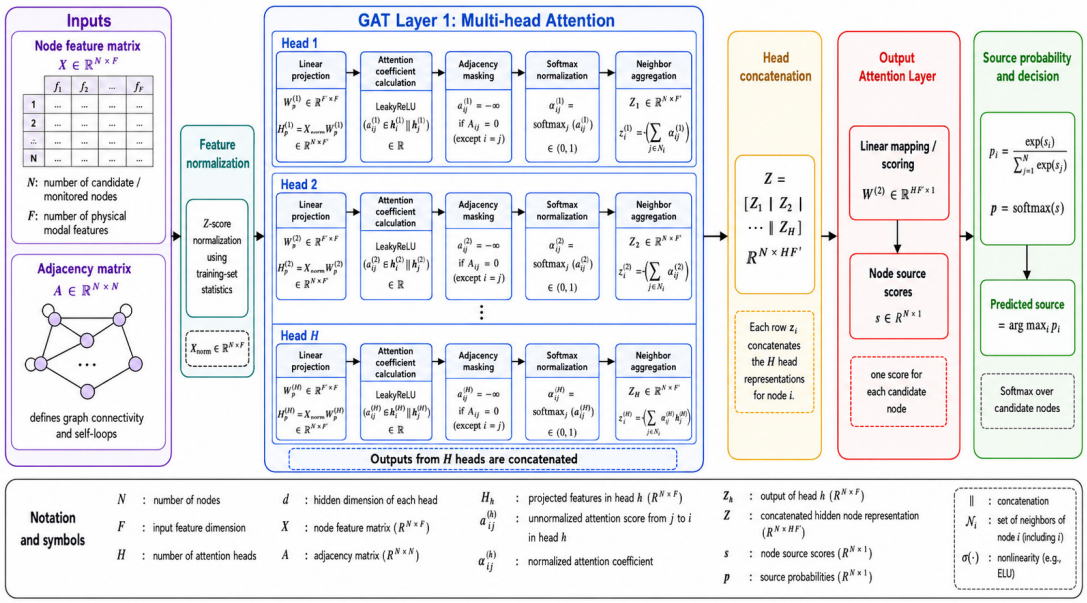


Figure 4. Detailed structural diagram of the proposed GAT framework.

3.3. Oscillation Source Localization Procedure

Based on the identification of Sub/Super-SO modal parameters from synchrophasor data, this section proposes an oscillation source localization method based on physical feature embedding and graph attention networks (GATs). In this approach, the identified oscillation modal parameters are embedded as physical features of nodes in a graph model, and the propagation of oscillation energy over the power grid topology is characterized through the attention mechanism. Consequently, accurate localization of oscillation sources can be achieved. The overall workflow of the proposed Sub/Super-SO source localization algorithm for power systems is illustrated in Figure 5.

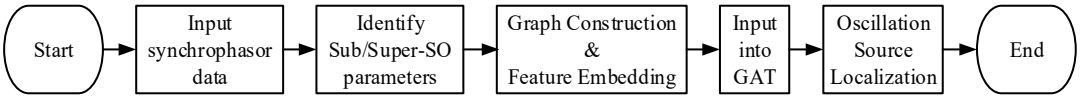


Figure 5. Oscillation source localization algorithm process.

1. Acquire generator terminal voltage/current synchrophasors from the WAMS;
2. Analyze the synchrophasor data using the modal parameter identification method proposed in Section 1. If oscillations are detected, decouple the Sub/Super-SO components and further identify key modal parameters, including frequency, amplitude, damping factor, and phase;
3. Construct the power system topology graph and embed the identified modal parameters as physical feature vectors into the graph nodes;
4. Use the GAT to adaptively aggregate neighborhood information and learn the spatial distribution and propagation patterns of oscillation features over the topology. Finally, compute the posterior probability of each node being the oscillation source to achieve localization.

4. Case Studies

4.1. Verification of the Identification Algorithm

To validate the effectiveness of the proposed Sub/Super-SO source localization algorithm, an improved IEEE 14-bus system was employed for analysis in MATLAB/Simulink R2020b The topology of the simulation system is shown in Figure 6.

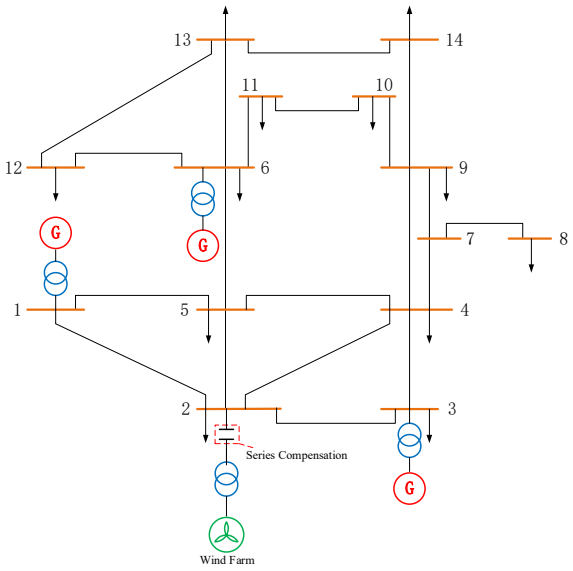


Figure 6. Improved IEEE 14-bus simulation model.

The system consists of 14 buses, 17 branches, and four generators located at buses 1, 2, 3, and 6. The steady-state generator parameters at buses 1, 3, and 6, as well as the line parameters of the model, are listed in Tables 1 and 2, respectively.

Table 1. Parameters of the generators in the IEEE 14 system.

Node	P/MW	Q/Mvar	Vg/pu
1	232.4	−16.9	1.06
3	0	23.4	1.01
6	0	12.2	1.07

Table 2. Parameters of the lines in the IEEE 14-bus system.

From Node	To Node	*r*/pu	*x*/pu	*b*/pu
1	2	0.01938	0.05917	0.0528
1	5	0.05403	0.22304	0.0492
2	3	0.04699	0.19797	0.0438
2	4	0.05811	0.17632	0.034
2	5	0.05695	0.17388	0.0346
3	4	0.06701	0.17103	0.0128
4	5	0.01335	0.04211	0
4	7	0	0.20912	0
4	9	0	0.55618	0
5	6	0	0.25202	0
6	11	0.09498	0.1989	0
6	12	0.12291	0.25581	0
6	13	0.06615	0.13027	0
7	8	0	0.17615	0
7	9	0	0.11001	0
9	10	0.03181	0.0845	0
9	14	0.12711	0.27038	0
10	11	0.08205	0.19207	0
12	13	0.22092	0.19988	0
13	14	0.17093	0.34802	0

Within the IEEE 14-bus simulation framework, a 100 MW doubly-fed induction generator (DFIG) wind turbine is connected to bus 2 through a filter. The corresponding wind farm parameters are summarized in Table 3.

Table 3. Doubly-fed wind farm parameters.

System Voltage	220 kV
Equivalent System Impedance, X_{system}	24.2 Ω
Transmission Line Inductance, L	0.78 H
Transmission Line Resistance, R	9.68
Initial Series Compensation, C (15%)	87.7 μF
Transformer Ratio	220 kV/690 V

An initial wind speed of 10 m/s is assigned to the wind turbine, and the transmission line is configured with a series compensation level of 15%. At t = 1 s, the series compensation level is suddenly increased to 60%. At the wind turbine terminal, instantaneous A-phase current data are sampled at a frequency of 10 kHz. The corresponding waveform is shown in Figure 7, and its amplitude variation is illustrated in Figure 8.

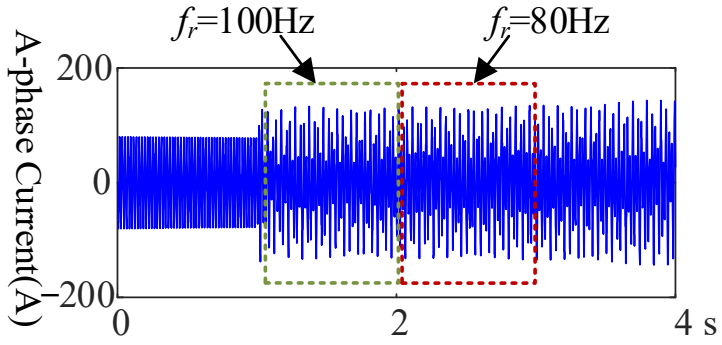


Figure 7. Instantaneous waveform of A-phase current.

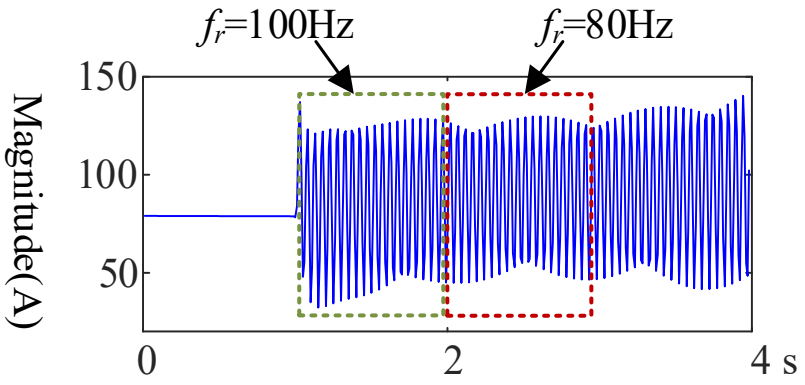


Figure 8. Synchronous phasor magnitude.

By exploiting the rotational characteristics of synchrophasors, an iterative matrix is constructed to decouple the Sub/Super-SO components in the synchrophasor, and the magnitudes of the solutions are then calculated. The results of $|A_0(m)H_{01}|$, $|A_1(m)H_{11}|$, $|A_2(m)H_{21}|$ are shown in Figure 9.

As shown in Figure 9, the magnitude of the Sub-SO component $|A_1(m)H_{11}|$ is significantly larger than that of the Super-SO component $|A_2(m)H_{21}|$, indicating that the oscillation is dominated by the sub-synchronous component. Furthermore, by taking the logarithm of $|A_0(m)H_{01}|$, $|A_1(m)H_{11}|$, $|A_2(m)H_{21}|$ and performing curve fitting, the

damping factors of each component can be obtained. Subsequently, combining the identified frequency f and damping factor α, H_{i1} is calculated, and the amplitudes of each component are determined. The identification results are presented in Table 4, which shows that the amplitude of the super-synchronous component is significantly smaller than that of the sub-synchronous component in this case. In addition, the results obtained by the proposed method are compared with those of the methods in [27,28]. The reference values are derived by applying the Hilbert–Huang transform (HHT) to the fault recording data within the interval of 2–3 s.

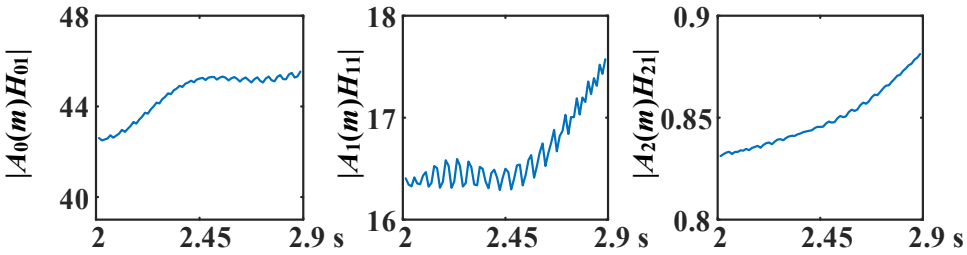


Figure 9. The magnitude of the solution obtained from a system of linear equations.

Table 4. Modal parameter identification results.

	Mode		A/A	f/Hz	α	θ
Case	Mode 1	Theoretical	32.2120	33.570	0.239	0.139π
		Identified	32.3430	33.571	0.238	0.138π
		Ref. [27]	33.1980	33.495	0.235	-
		Ref. [28]	33.0976	33.475	0.240	-
	Mode 2	Theoretical	1.4896	66.432	0.016	-0.276π
		Identified	1.4926	66.431	0.015	-0.276π
		Ref. [27]	-	-	-	-
		Ref. [28]	-	-	-	-

The comparative analysis shows that the proposed method yields identification results closer to the theoretical values than those reported in [27,28]. This is because the reporting rate f_r = 100 Hz does not satisfy the Nyquist sampling theorem, causing the Super-SO component to undergo spectral shifting and aliasing with the Sub-SO spectrum. As a result, the Sub-SO amplitudes obtained by the methods in [27,28] are overestimated relative to the theoretical values. In contrast, the proposed method not only distinguishes the presence of Sub/Super-SO components, but also accurately identifies their modal parameters.

4.2. Verification of the Localization Method

Based on the completed oscillation modal parameter identification, the effectiveness of the GAT-based oscillation source localization method with physical feature embedding proposed in Section 2 is further validated under complex network conditions.

First, according to the graph construction method proposed in this paper, the power system is modeled as a graph $G = (V, E)$. The node set V represents the bus nodes in the system and is defined as:

$$V = (v_1, v_2, \ldots, v_{14}) \tag{15}$$

Each transmission line is abstracted as an undirected edge. If a physical connection exists between node i and node j, an edge is introduced in the graph:

$$E = \{e_{ij} | Nodes\ i\ and\ j\ are\ physically\ connected\} \tag{16}$$

According to the topology of the IEEE 14-bus system, a total of 17 undirected edges are constructed. Accordingly, the adjacency matrix $\boldsymbol{A}_{\text{adj}}$ of the test system graph is given by:

$$\boldsymbol{A}_{adj} = \begin{bmatrix} 0 & 1 & 0 & 0 & 1 & 0 & 0 & 0 & 0 & 0 & 0 & 0 & 0 & 0 \\ 1 & 0 & 1 & 1 & 1 & 0 & 0 & 0 & 0 & 0 & 0 & 0 & 0 & 0 \\ 0 & 1 & 0 & 1 & 0 & 0 & 0 & 0 & 0 & 0 & 0 & 0 & 0 & 0 \\ 0 & 1 & 1 & 0 & 1 & 0 & 0 & 0 & 0 & 0 & 0 & 0 & 0 & 0 \\ 1 & 1 & 0 & 1 & 0 & 0 & 0 & 0 & 0 & 0 & 0 & 0 & 0 & 0 \\ 0 & 0 & 0 & 0 & 0 & 0 & 0 & 0 & 0 & 0 & 1 & 1 & 1 & 0 \\ 0 & 0 & 0 & 0 & 0 & 0 & 0 & 1 & 1 & 0 & 0 & 0 & 0 & 0 \\ 0 & 0 & 0 & 0 & 0 & 0 & 1 & 0 & 0 & 0 & 0 & 0 & 0 & 0 \\ 0 & 0 & 0 & 0 & 0 & 0 & 1 & 0 & 0 & 1 & 0 & 0 & 0 & 1 \\ 0 & 0 & 0 & 0 & 0 & 0 & 0 & 0 & 1 & 0 & 1 & 0 & 0 & 0 \\ 0 & 0 & 0 & 0 & 0 & 1 & 0 & 0 & 0 & 1 & 0 & 0 & 0 & 0 \\ 0 & 0 & 0 & 0 & 0 & 1 & 0 & 0 & 0 & 0 & 0 & 0 & 1 & 0 \\ 0 & 0 & 0 & 0 & 0 & 1 & 0 & 0 & 0 & 0 & 0 & 1 & 0 & 1 \\ 0 & 0 & 0 & 0 & 0 & 0 & 0 & 0 & 1 & 0 & 0 & 0 & 1 & 0 \end{bmatrix} \tag{17}$$

The constructed adjacency matrix describes the static topological structure of the power grid.

Then, to enable oscillation source localization, ideal PMU models are installed at buses 1, 2, 3, and 6. Although the modified IEEE 14-bus system contains 14 buses, the GAT-based localization model in this case is constructed only on the measured candidate buses. Therefore, buses 1, 2, 3, and 6 are selected as the candidate oscillation source nodes for the GAT localization task. The unmeasured buses are excluded from the candidate-node feature matrix in this case.

Different oscillation scenarios are simulated by varying the connection point of the DFIG and the level of series compensation. For each scenario, synchrophasor data of terminal voltages and currents over 1–4 s are recorded, from which the Sub-SO modal parameters of each phase at the four buses are identified on a per-second basis. A total of 1000 samples is obtained, and Gaussian white noise with a signal-to-noise (SNR) ratio of 30 dB is added to the generated synchrophasor data to simulate measurement noise in practical PMU systems. The dataset is divided into training, validation, and test sets in a ratio of 7:1:2 using stratified sampling. The validation set is used for learning-rate scheduling and early stopping, while the test set is used only for final performance evaluation. To make the GAT-based localization experiment reproducible, the main hyperparameter settings of the proposed model are summarized in Table 5.

The identified modal parameters, including frequency, amplitude, damping factor, and phase, are assembled into physical feature vectors and embedded into the corresponding graph nodes. The constructed graph structure and node feature matrix are then fed into the trained GAT model for forward inference.

The GAT model employs a multi-head attention mechanism and incorporates adjacency matrix information to adaptively aggregate physical features from neighboring nodes. By computing the attention coefficients e_{ij} between nodes, the model captures the propagation and distribution patterns of oscillation energy over the network topology. Fi-

nally, after Softmax normalization at the output layer, the posterior probability distribution of each node being the oscillation source is obtained, as shown in Figure 10.

Table 5. Hyperparameter settings of the proposed GAT model.

Hyperparameter	Setting
Number of samples	1000
Candidate source nodes	4
Input feature matrix	$X \in \mathbb{R}^{14\times3}$
Input features	Damping factor, amplitude, phase
Data split	Training/validation/test = 7:1:2
Number of GAT layers	2
Attention heads	4 in the first layer and 1 in the output layer
Hidden dimension	8 per attention head
Weight matrix of the first layer	$W^{(1)} \in \mathbb{R}^{3\times8}$ for each head
Weight matrix of the output layer	$W^{(2)} \in \mathbb{R}^{32\times1}$
Attention activation	LeakyReLU, negative slope = 0.2
Hidden-layer activation	ELU
Output function	Softmax
Dropout rate	0.2
Loss function	Cross-entropy loss
Optimizer	Adam
Initial learning rate	0.01
Learning-rate schedule	Reduce by a factor of 0.5 if the validation loss does not improve for 20 epochs
Minimum learning rate	10^{-5}
Batch size	32
Maximum epochs	500
Normalization strategy	Z-score normalization using training-set statistics
Early stopping criterion	Stop if the validation loss does not improve by more than 10^{-4} for 50 epochs
Random seed	123
Computational cost	$O(HNFd + H^2d)$, where H denotes the number of attention heads, N denotes the number of nodes, F denotes the input feature dimension of each node, and d denotes the hidden feature dimension of each attention head.

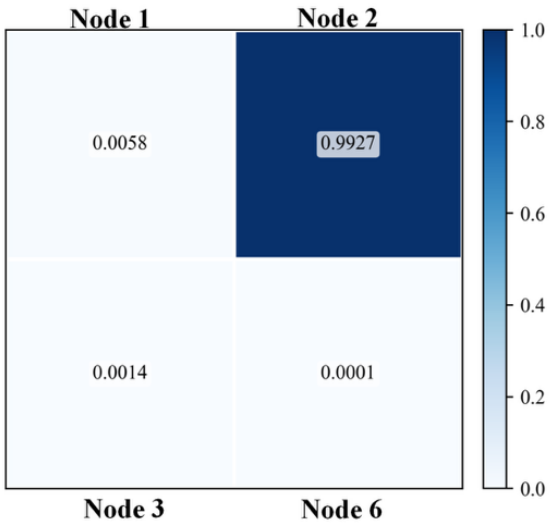


Figure 10. Probability of each unit being the oscillation source.

As shown in the probability distribution in Figure 10, the GAT model assigns the highest probability to node 2 as the oscillation source, which is fully consistent with the actual fault location set in the simulation. This result indicates that the model successfully captures the distinctive physical characteristics exhibited by node 2. During the graph attention aggregation process, higher attention weights are assigned to its neighboring connections, thereby significantly amplifying its influence within the network and enabling accurate localization. The process is shown in Figure 11.

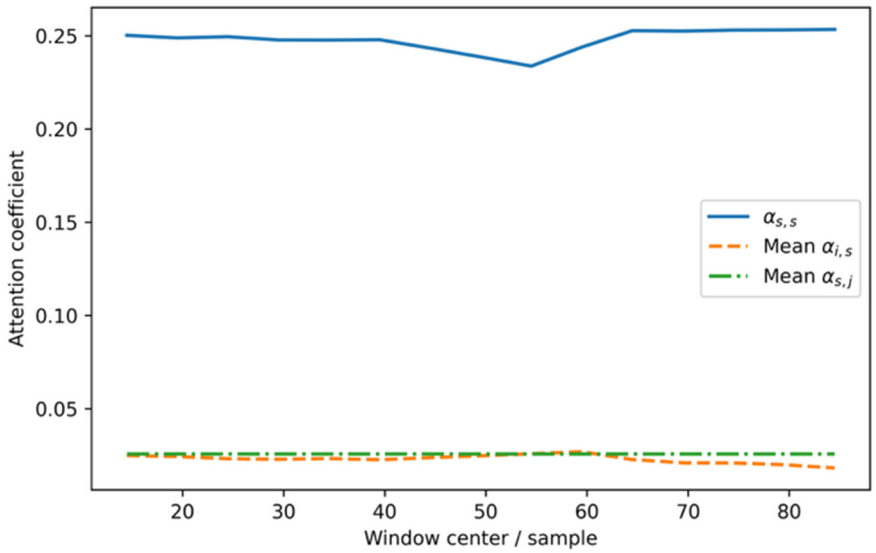


Figure 11. Dynamic trajectory of attention coefficients over consecutive sliding time windows.

To avoid relying only on a single localization probability result, the localization performance is further evaluated under different oscillation source scenarios. The test samples are grouped according to the actual oscillation source node, and the number of test samples, correctly localized samples, and localization accuracy are reported in Table 6. These results provide direct quantitative evidence for the localization performance of the proposed method under different source-location conditions.

Table 6. Localization accuracy under different oscillation source scenarios.

Source Node	Accuracy (%)
1	99.29
2	99.30
3	99.28
6	99.26

4.3. Robustness and Comparative Validation on the IEEE 39-Bus System

To further verify the scalability and robustness of the proposed oscillation source localization method, the IEEE-39 bus system shown in Figure 12 was considered in the case studies. Compared with the modified IEEE 14-bus system used in the previous subsection, this system contains more buses and a more complex network topology. Therefore, it provides a more challenging benchmark for evaluating whether the proposed GAT-based localization model can remain effective under a larger-scale network structure. This dataset simulates different oscillation scenarios by varying the control parameters and grid-connection buses of renewable energy stations, which contains 814 oscillation scenarios.

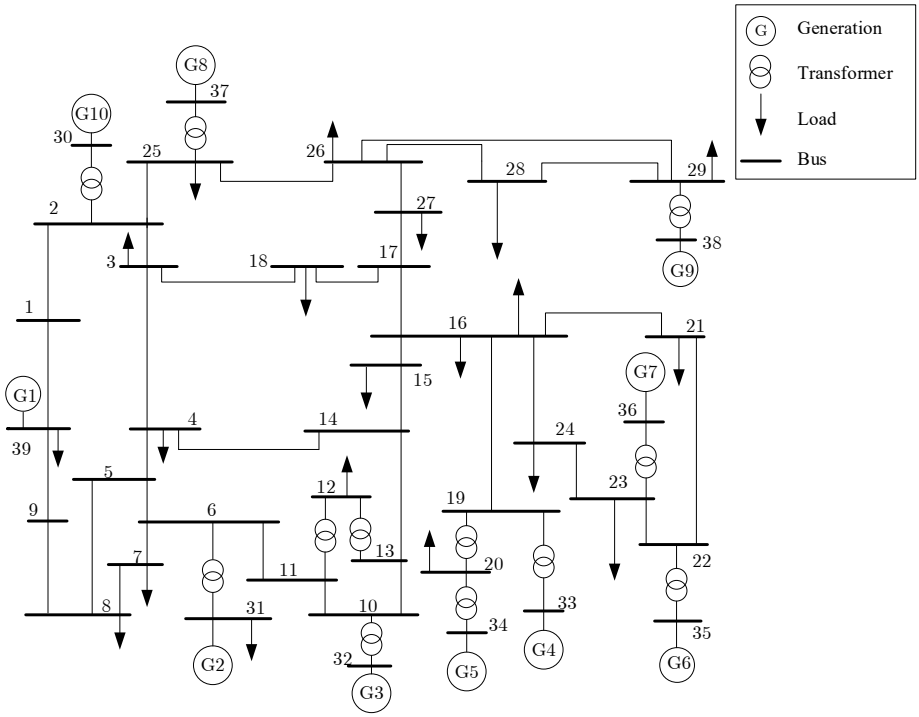


Figure 12. Schematic diagram of the IEEE-39 bus system.

In this test, oscillation scenarios are generated on the IEEE 39-bus system, and the corresponding node signals are used as the input of the proposed localization model. To simulate non-ideal PMU measurement conditions, Gaussian white noise is added to the input time-series data under different SNR levels, including 20 dB, 30 dB, 40 dB, and 50 dB. The clean-data case is also tested as a reference. The localization results under different SNR levels are summarized in Table 7.

Table 7. Localization accuracy under different SNR levels.

SNR Level	Accuracy (%)
Clean	100.00
20 dB	87.80
30 dB	99.02
40 dB	99.51
50 dB	99.99

As shown in Table 7, the proposed method achieves 100.00% localization accuracy in the clean-data case. When the SNR decreases to 20 dB, the localization accuracy decreases to 87.80%, because this condition corresponds to the strongest measurement noise among the tested cases. The stronger noise disturbance may distort the oscillation waveform and weaken the distinguishability of source-related node features. Nevertheless, the proposed method still maintains acceptable localization performance under the severe 20 dB noise condition. When the SNR increases to 30 dB and above, the localization accuracy recovers to more than 99%, indicating that the proposed method has good robustness under moderate and high-quality PMU measurement conditions.

To validate the superiority of the proposed oscillation source localization method, it was compared with the following two representative methods:

1. LSTM-based localization method: The synchrophasor time-series data of each node are directly fed into a long short-term memory (LSTM) network, and its tem-

poral modeling capability is utilized to perform oscillation source classification and localization.

2. GAT-based localization without parameter identification: Without performing the modal parameter identification described in Section 1, the raw synchrophasor magnitudes are directly used as node features and fed into the GAT model, where localization is achieved based on the graph structure.

To ensure a fair comparison, all methods used the same training and test set partition, the same IEEE 39-bus simulation system and oscillation scenarios, and Gaussian white noise with an SNR ratio of 30 dB was uniformly added to simulate practical measurement conditions. The number of training epochs for all three oscillation source localization methods was set to 200, and each method was independently trained and tested five times using different random initializations. The mean accuracy, standard deviation, best accuracy, worst-case accuracy, precision, recall, and F1-score are reported under the same dataset split and noise condition. The test accuracy results are presented in Table 8.

Table 8. Performance comparison of different localization methods.

Method	Acc. (%)	Acc. Std. (%)	Best Acc. (%)	Worst Acc. (%)	Precision (%)	F1-Score (%)
Proposed Method	99.02	0.18	99.77	98.78	99.52	99.51
LSTM-based localization method	98.14	0.13	98.54	98.10	98.10	98.08
GAT without parameter identification	98.57	0.12	99.07	98.54	98.54	98.53

As shown in Table 8, the proposed method outperforms the comparison methods across all evaluation metrics. Compared with the LSTM-based method, the proposed approach not only captures the spatial correlations among nodes through the graph structure, but also enhances the interpretability and robustness of the input features via physical feature embedding, thereby significantly improving localization accuracy.

Compared with the GAT method without parameter identification, the proposed approach effectively extracts key oscillation features through modal parameter identification. This enables the GAT model to more accurately focus on the propagation patterns of oscillation sources and avoids the negative impact of high-dimensional redundant raw data on model training.

5. Conclusions

This paper investigated the wide-area monitoring and localization of Sub/Super-SO in power-electronics-dominated power systems. The main conclusions are as follows:

A high-precision Sub/Super-SO detection and modal parameter identification method based on synchrophasors is proposed. By adjusting the order of the Vandermonde matrix constructed from rotation factors, the method effectively resolves the spectral aliasing issue, enabling decoupling and the accurate identification of oscillation modal parameters.

An oscillation source localization method based on physical feature embedding and graph attention networks is proposed. This method integrates the physical interpretability of system dynamics with the graph learning capability of deep learning: high-precision modal parameters are embedded as node features, and the attention mechanism of GAT is utilized to adaptively learn the propagation patterns of oscillation energy over the power grid topology.

Simulation results on the modified IEEE 14 and 39-bus system demonstrate that the proposed method not only achieves higher identification accuracy than conventional approaches, but also enables effective aggregation of critical node features in the localization stage using the GAT model. This results in high-confidence localization outputs and

accurate online identification of Sub/Super-SO sources, providing a new technical support for stability analysis and the control of modern power systems.

Author Contributions: Conceptualization, B.D. and R.Y.; methodology, L.Y. and S.G.; software, B.D. and J.L. (Jiajian Lin); validation, B.D., R.Y. and J.L. (Jianghui Li); formal analysis, B.D. and R.Y.; investigation, B.D.; resources, J.L. (Jianghui Li) and J.L. (Jiajian Lin); data curation, C.G.; writing—original draft preparation, R.Y., B.D. and L.Y.; writing—review and editing, L.Y. and S.G.; supervision, B.D. and R.Y.; and project administration, B.D. All authors have read and agreed to the published version of the manuscript.

Funding: This research was funded by Science and Technology Project of State Grid Corporation of China (Grant: B3130N25Z007).

Data Availability Statement: The data that support the findings of this study are available from the corresponding author, S.G., upon reasonable request.

Conflicts of Interest: Authors Buqing Deng, Rong Ye, Jianghui Li, Jiajian Lin, and Chenhao Guan were employed by the company State Grid Fujian Electric Power Co., Ltd. Economic and Technical Research Institute. The authors declare that this study received funding from Science and Technology Project of State Grid Corporation of China, grant number B3130N25Z007. The funder had the following involvement with the study: study design, collection, analysis, interpretation of data, the writing of this article or the decision to submit it for publication. The remaining authors declare that the research was conducted in the absence of any commercial or financial relationships that could be construed as potential conflicts of interest.

References

1. Hossain, M.I.; Hamanah, W.M.; Alam, M.S.; Shafiullah, M.; Abido, M.A. Fault Ride Through and Intermittency Improvement of Renewable Energy Integrated MMC-HVDC System Employing Flywheel Energy Storage. *IEEE Access* **2023**, *11*, 50528–50546. [CrossRef]
2. Shi, Z.; Wang, W.; Huang, Y.; Li, P.; Dong, L. Simultaneous Optimization of Renewable Energy and Energy Storage Capacity with the Hierarchical Control. *CSEE J. Power Energy Syst.* **2022**, *8*, 95–104. [CrossRef]
3. Xie, X.; Sun, Y. A piecewise probabilistic harmonic power flow approach in unbalanced residential distribution systems. *Int. J. Electr. Power Energy Syst.* **2022**, *141*, 108114. [CrossRef]
4. Shair, J.; Li, H.; Hu, J.; Xie, X. Power System Stability Issues, Classifications and Research Prospects in the Context of High-Penetration of Renewables and Power Electronics. *Renew. Sustain. Energy Rev.* **2021**, *145*, 111111. [CrossRef]
5. Zhang, Z.; Kou, P.; Mei, M.; Tian, R.; Zhang, Y.; Liang, D. Interaction Analysis and Damping Control of Sub-Synchronous Oscillation and Medium-Frequency Oscillation in HVDC-Connected Offshore Wind Farm. *IEEE Trans. Power Syst.* **2025**, *40*, 4336–4352. [CrossRef]
6. Xie, X.; Zhan, Y.; Shair, J.; Ka, Z.; Chang, X. Identifying the Source of Subsynchronous Control Interaction via Wide-Area Monitoring of Sub/Super-Synchronous Power Flows. *IEEE Trans. Power Deliv.* **2019**, *35*, 2177–2185. [CrossRef]
7. Zhu, J.; Hu, J.; Lin, L.; Wang, Y.; Wei, C. High-Frequency Oscillation Mechanism Analysis and Suppression Method of VSC-HVDC. *IEEE Trans. Power Electron.* **2020**, *35*, 8892–8896. [CrossRef]
8. Ma, J.; Su, N.; Deng, Y.; Xia, W.; Xu, H.; Shen, Y. Oscillation Suppression Considering Characteristics of Interaction Energy in Grid-Connected DFIG-Based Wind Farms via VSC-HVDC Transmission System. *J. Mod. Power Syst. Clean. Energy* **2025**, *13*, 698–709. [CrossRef]
9. Gao, Y.; Gao, S.; Guo, C. Numerical Oscillation Suppression of Electromagnetic Transient Simulation Based on Eigenvalue Analysis. In Proceedings of the IEEE PES 16th Asia-Pacific Power and Energy Engineering Conference (APPEEC), Nanjing, China, 25–27 October 2024; pp. 1–5. [CrossRef]
10. Goldstein, A.; Maragal, D. Synchrophasor Measurement System Industry Standards and Guidance: A Comprehensive Overview. *IEEE Trans. Power Deliv.* **2024**, *39*, 1687–1696. [CrossRef]
11. Gao, S.; Chen, Y.; Yu, Z.; Cao, T.; Chen, W.; Song, Y.; Wang, Y. An interface method for co-simulation of EMT model and shifted frequency EMT model based on estimation of signal parameters via rotational invariance techniques. *IEEE Trans. Power Syst.* **2025**, *40*, 3576–3579. [CrossRef]
12. Zhang, X.; Zhang, F.; He, J.; Gao, W. An enhanced matrix pencil method for parameter identification of sub-/super-synchronous oscillations using synchrophasors. *IEEE Trans. Ind. Inform.* **2025**, *21*, 1684–1693. [CrossRef]

13. Wang, L.; Zhang, Z.; Sun, Z.; Gao, H.; Jiang, S.; Xia, S.; Lie, T.T. Synchrophasor-Based Parameter Identification of Sub/Super-Synchronous Oscillations Using Adaptive Empirical Fourier Decomposition. *IEEE Trans. Power Deliv.* **2026**, *41*, 423–436. [CrossRef]
14. Zhang, F.; Li, J.; Liu, J.; Gao, W.; He, J. An Improved Interpolated DFT-Based Parameter Identification for Sub-/Super-Synchronous Oscillations with Synchrophasors. *IEEE Trans. Power Syst.* **2023**, *38*, 1714–1727. [CrossRef]
15. Wei, Z.; Wu, Y.; Lin, Q.; Zhang, P. Online Detection and Location Scheme for Aged Cable Segment in MMC-HVDC Systems Based on Admittance Spectrum and Compressed Sensing. *IEEE Trans. Ind. Inform.* **2024**, *20*, 13831–13841. [CrossRef]
16. Xu, Y.; Zhu, A.; Cheng, Y. An Adaptive-Parameter-Based Master-Slave Suppression Strategy for Subsynchronous Oscillations in Wind Power Grid-Connected Systems. In Proceedings of the 2025 IEEE International Conference on Power and Integrated Energy Systems (ICPIES), Haikou, China, 7–9 April 2025; pp. 70–75. [CrossRef]
17. Zhang, Z.; Zhao, H.; Zhang, M.; Liu, Y.; Wang, Y. Research on sub-synchronous-oscillation energy analysis and traceability method based on refined energy. *Energies* **2024**, *17*, 1683. [CrossRef]
18. Jiang, T.; Liu, B.; Li, X.; Mazza, A.; Li, G.; Pons, E.; Huang, T. Subsynchronous oscillation source location in power system with high penetration of wind power using multivariate variational mode decomposition. *IEEE Trans. Power Syst.* **2025**, *40*, 4971–4982. [CrossRef]
19. Liu, R.; Zhang, Y.; Gao, S.; Li, D.; Liu, C.; Che, J.; Tian, R.; Song, Y. Localization of forced oscillation sources in power systems with grid-forming wind turbines based on ICEEMDAN-ITEO. *Energies* **2025**, *18*, 6025. [CrossRef]
20. Gao, J.; Yang, Y.; Xu, H.; Xie, Y.; Zhou, C.; Dong, H. The wideband oscillatory localization method based on combining compressed sensing and graph attention networks. *Energies* **2024**, *17*, 6062. [CrossRef]
21. Zhang, Y.; Liu, Y.; Zheng, Z.; Gao, S. A wideband oscillation classification method based on multimodal feature fusion. *Electronics* **2026**, *15*, 682. [CrossRef]
22. Chen, H.; Gao, S.; Zhou, X.; Chen, Y.; Zheng, Z.; Wang, Y.; Zhai, B. Deep reinforcement learning-based time-varying parameter identification method for grid-connected renewable power generation systems. *IEEE Trans. Sustain. Energy* **2025**, *17*, 2219–2232. [CrossRef]
23. Huang, T.; Freris, N.M.; Kumar, P.R.; Xie, L. A Synchrophasor Data-Driven Method for Forced Oscillation Localization under Resonance Conditions. *IEEE Trans. Power Syst.* **2020**, *35*, 3927–3939. [CrossRef]
24. Frigo, G.; Pegoraro, P.A.; Toscani, S. PMU Algorithms Based on Adaptive Taylor-Fourier Models: A Three-Phase Compressive Sensing Method for Spectral Support Recovery. *IEEE Trans. Instrum. Meas.* **2025**, *74*, 9003014. [CrossRef]
25. Frigo, G.; Pegoraro, P.A.; Toscani, S. Enhanced Support Recovery for PMU Measurements Based on Taylor-Fourier Compressive Sensing Approach. *IEEE Trans. Instrum. Meas.* **2022**, *71*, 9004211. [CrossRef]
26. Liu, S.; Zhao, Y.; Lin, Z.; Liu, Y.; Ding, Y.; Yang, L.; Yi, S. Data-Driven Event Detection of Power Systems Based on Unequal-Interval Reduction of PMU Data and Local Outlier Factor. *IEEE Trans. Smart Grid* **2019**, *11*, 1630–1643. [CrossRef]
27. Yang, X.; Zhang, J.; Xie, X.; Xiao, X.; Gao, B.; Wang, Y. Interpolated DFT-based identification of sub-synchronous oscillation parameters using synchrophasor data. *IEEE Trans. Smart Grid* **2020**, *11*, 2662–2675. [CrossRef]
28. Wang, Y.; Chao, M.; Xie, X.; Jiang, X.; Song, Z. Identification of subsynchronous oscillation parameters and field tests based on PMU data. *Proc. CSEE* **2022**, *42*, 899–908. [CrossRef]

Disclaimer/Publisher's Note: The statements, opinions and data contained in all publications are solely those of the individual author(s) and contributor(s) and not of MDPI and/or the editor(s). MDPI and/or the editor(s) disclaim responsibility for any injury to people or property resulting from any ideas, methods, instructions or products referred to in the content.